Pi2 pulsations associated with poleward boundary intensifications during the absence of substorms

K.-H. Kim,[1] K. Takahashi,[2] D.-H. Lee,[1] P. R. Sutcliffe,[3] and K. Yumoto[4]

Received 7 September 2004; revised 22 October 2004; accepted 17 November 2004; published 28 January 2005.

[1] Pi2 pulsations during the intervals of extremely quiet geomagnetic conditions ($Kp = 0$) have been reported by *Sutcliffe and Lyons* [2002]. These authors observed that several Pi2 bursts occurred simultaneously at high (magnetic latitude = 71°) and low (42°) latitudes during the absence of magnetospheric substorms and found that the bursts are strongly correlated with poleward boundary intensifications (PBIs). The authors discussed the correlation between the PBI-associated Pi2 (PBI-Pi2) bursts and enhancements of energetic particle fluxes in the plasma sheet, but they did not focus on the wave properties of the PBI-Pi2 pulsations. In this study we examine whether the PBI-Pi2 pulsations at middle/low latitudes exhibit spatial variations similar to substorm-associated Pi2 pulsations. Using ground-based data from latitudinally and longitudinally extended magnetometer network and spacecraft data in the duskside, we investigate the spatial variation of the frequency, amplitude, phase, and interstation coherence of the PBI-Pi2 events. We show that the PBI-Pi2 pulsations in this study have different features at different local times and suggest that their period and duration are determined at a source region, where fast earthward flows brake.

Citation: Kim, K.-H., K. Takahashi, D.-H. Lee, P. R. Sutcliffe, and K. Yumoto (2005), Pi2 pulsations associated with poleward boundary intensifications during the absence of substorms, *J. Geophys. Res.*, *110*, A01217, doi:10.1029/2004JA010780.

1. Introduction

[2] Pi2 magnetic pulsations have been commonly observed at the onset of a magnetospheric substorm. They are damped and transient geomagnetic oscillations with periods of 40–150 s [e.g., *Saito*, 1969]. Magnetic pulsations in the Pi2 band occur at all latitudes on the nightside and exhibit latitudinal and longitudinal variations in amplitude and phase [*Yumoto*, 1986].

[3] The amplitude of Pi2 pulsations maximizes at high latitudes. High-latitude Pi2 pulsations are mainly observed in the region of substorm-enhanced ionospheric electrojet [e.g., *Olson and Rostoker*, 1975]. The evolution of these pulsations is tied to the evolution of the substorm current system. Midlatitude/low-latitude Pi2 pulsations have different spectral contents from those at high latitude, suggesting different source mechanism for different latitudes [*Yumoto et al.*, 1994]. The excitation mechanisms of the midlatitude/low-latitude Pi2 have been considered as shear Alfvén mode resonances [*Fukunishi*, 1975], surface waves on the plasmapause [*Sutcliffe*, 1975], and cavity mode resonances [*Saito and Matsushita*, 1968]. Such models for the lower-latitude Pi2 have been well organized by *Yeoman and Orr* [1989] and by *Osaki et al.* [1998]. Ground-based observations [e.g., *Stuart*, 1974; *Yeoman and Orr*, 1989; *Lin et al.*, 1991] and ground-satellite observations [e.g., *Takahashi et al.*, 1995; *Takahashi et al.*, 2001; *Kim et al.*, 2001; *Keiling et al.*, 2001] showed that the cavity mode in the plasmasphere, which is driven by impulsive source outside the plasmapause, is a promising mechanism for low-latitude to midlatitude Pi2 pulsations.

[4] Recently, it has been proposed that Pi2 is generated by compressional pulses produced by high-speed earthward flows in the near-tail [*Shiokawa et al.*, 1998; *Kepko and Kivelson*, 1999]. That is, Pi2 pulsations in the inner magnetosphere can be directly driven by oscillatory sources external to the plasmapause. *Osaki et al.* [1998] suggested that Pi2 pulsations observed off the magnetic equator in the plasmasphere are not a simple cavity mode oscillation excited by an impulsive source. *Shiokawa et al.* [1998] reported that substorm-associated high-speed flow burst was followed by a Pi2 pulsation that is observed both in the inner magnetosphere and on the ground. *Kepko and Kivelson* [1999] and *Kepko et al.* [2001] showed several examples of Pi2 waves and flow oscillations that have nearly identical waveforms. The authors suggested that flows in the magnetotail determine the properties of the low-latitude Pi2 pulsations.

[5] Substorms are not the only phenomenon associated with high-speed earthward flows and Pi2 pulsations. *Lyons et al.* [1999] studied a type of geomagnetic activity termed poleward boundary intensifications (PBIs). PBIs are night-

[1]Department of Astronomy and Space Science, Kyung Hee University, Kyunggi, Korea.
[2]Johns Hopkins University Applied Physics Laboratory, Laurel, Maryland, USA.
[3]Hermanus Magnetic Observatory, Hermanus, South Africa.
[4]Space Environment Research Center, Kyushu University, Fukuoka, Japan.

0148-0227/05/2004JA010780$09.00

Table 1. List of International Monitor for Auroral Geomagnetic Effects (IMAGE) (Ny Ålesund (NAL)-Muonio (MUO)) and Sub-Auroral Magnetometer Network (SAMNET) (Oulu (OUL)-York (YOR)) Stations

		Geographic		Corrected Geomagnetic	
Station	Code	Latitude	Longitude	Latitude	Longitude
Ny Ålesund	NAL	78.92°	11.95°	76.08°	112.36°
Longyearbyen	LYR	78.20°	15.82°	75.13°	113.14°
Hornsund	HOR	77.00°	15.60°	74.03°	110.58°
Hopen Island	HOP	76.51°	25.01°	72.92°	116.00°
Bear Island	BJN	74.50°	19.20°	71.35°	108.91°
Tromsø	TRO	69.66°	18.94°	66.56°	103.57°
Kilpisjärvi	KIL	69.02°	20.79°	65.80°	104.44°
Muonio	MUO	68.02°	23.53°	64.63°	105.81°
Oulu	OUL	65.10°	25.85°	61.54°	105.82°
Kvistaberg	KVI	59.50°	17.63°	56.03°	96.33°
York	YOR	53.95°	358.95°	50.97°	78.90°

side geomagnetic disturbances that have an auroral signature moving equatorward from the poleward boundary of the auroral zone. PBIs occur under all geomagnetic conditions, both in the presence and absence of substorms. *Lyons et al.* [1999] revealed that there were bursty flows in the plasma sheet during the PBIs and that each PBI accompanied a Pi2 pulsation. *Sutcliffe and Lyons* [2002] reported PBI-associated Pi2 pulsations, which occurred simultaneously at high (magnetic latitude = 71°) and low (42°) latitudes, during the absence of substorms. The authors discussed the relation between PBIs and energetic particle enhancements in the plasma sheet and between PBIs and Pi2-burst train. However, the physical properties and excitation mechanism of the PBI-associated Pi2 pulsations were not included in their discussion.

[6] In this study we focus on the PBI-associated Pi2 pulsations reported by *Sutcliffe and Lyons* [2002]. We examine whether the nonsubstorm Pi2 events exhibit spatial variations similar to substorm-related Pi2 pulsations and examine the characteristics of the PBI-related pulsations, using ground-based data and spacecraft data.

[7] The organization of the paper is as follows. In section 2 we briefly describe the data sets used in this study. In section 3 we describe the data analysis. In section 4 we compare our observations with previous studies and discuss the possible model for explaining the observations. Section 5 presents the conclusions.

2. Data Sets

[8] We use ground-based magnetometer data from the International Monitor for Auroral Geomagnetic Effects (IMAGE) [*Lühr et al.*, 1998], the Sub-Auroral Magnetometer Network (SAMNET) [*Yeoman et al.*, 1990], the Circum-pan Pacific Magnetometer Network (CPMN) [*Yumoto et al.*, 1996], and Hermanus (HER) station [*Sutcliffe and Yumoto*, 1989]. The geographic and corrected geomagnetic coordinates (CGM) are listed in Table 1 for SAMNET and IMAGE stations and Table 2 for HER and CPMN stations, respectively. The time resolutions of magnetometer data are 10 s for the IMAGE stations and 5 s for the SAMNET stations. The 5-s average data generated from the original 1-s samples are used for the CPMN and HER data.

[9] We compare the ground magnetic field data with the spin-averaged (∼6 s) electric field [*Harvey et al.*, 1995] and magnetic field [*Russell et al.*, 1995] data acquired at dusk (∼1800–1900 MLT) by the Polar spacecraft. The Polar magnetic field data have been rotated into mean field-aligned coordinates in which $\hat{e}_{zMFA}$ is along the averaged magnetic field defined by taking the 5-min boxcar running averages of the ∼6-s data, the azimuthal direction $\hat{e}_{yMFA}$ is parallel to $\hat{e}_{zMFA} \times \mathbf{r}$, where $\mathbf{r}$ is the spacecraft position vector with respect to the center of the Earth, and the radially outward component is given by $\hat{e}_{xMFA} = \hat{e}_{yMFA} \times \hat{e}_{zMFA}$. The electric field data will be presented using the spacecraft coordinates (56, *XY*, *Z*). The electric field vector was only determined from the measurements of two spin-plane components (i.e., E_{xy} and E_z). In the spacecraft coordinate system, $\hat{e}_z$ lies in the spacecraft spin plane, pointing approximately toward the ecliptic north, $\hat{e}_{xy}$ lies in the spin plane perpendicular to $\hat{e}_z$, pointing antisunward, and $\hat{e}_{56}$ completes a right-hand system (i.e., $\hat{e}_{xy} \times \hat{e}_z = \hat{e}_{56}$). The radial field oscillations can be identified in the *XY* and/or *Z* components with respect to the satellite location in the meridian plane. The azimuthal oscillation is in the

Table 2. List of Hermanus and Circum-Pan Pacific Magnetometer Network (CPMN) Stations

		Geographic		Corrected Geomagnetic	
Station	Code	Latitude	Longitude	Latitude	Longitude
Hermanus	HER	−34.45°	19.25°	−42.09°	82.42°
Tixie	TIK	71.59°	128.78°	65.78°	197.01°
Magadan	MGD	59.97°	150.86°	53.63°	218.93°
Popov Island	PPI	42.98°	131.73°	36.42°	203.84°
Kakioka	KAK	36.23°	141.19°	29.11°	212.49°
Yamakawa	YMK	31.19°	130.62°	24.24°	202.36°
Lunpin	LNP	25.00°	121.17°	18.05°	192.81°
Muntinlupa	MUT	14.37°	121.02°	3.58°	191.57°
Ancon	ANC	−12.08°	−77.02°	1.50°	354.41°

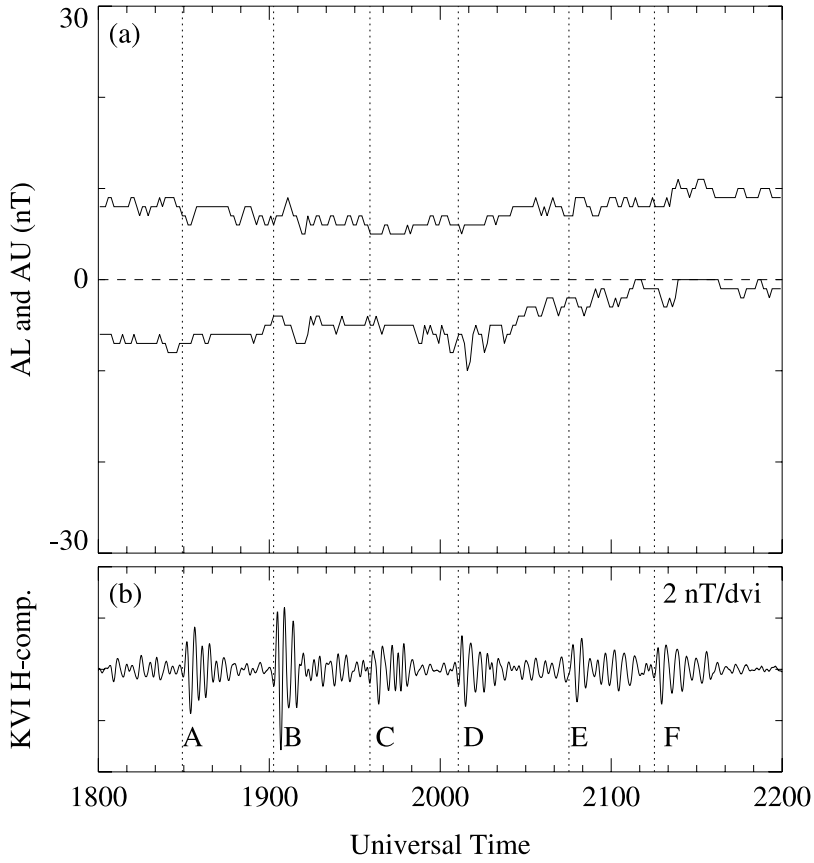

Figure 1. (a) Provisional auroral electrojet indices on 27 December 1997. (b) Filtered (4–10 mHz) *H*-component magnetic field perturbations at midlatitude Kvistaberg (KVI) station. The vertical dotted lines indicate the onset times of the poleward boundary intensification (PBI) -Pi2 bursts.

56 component. The 56 and *XY* components are azimuthal and radial components near the equator, respectively.

3. Analysis of PBI-Associated Pi2 Pulsations

[10] The 4-hour interval (1800–2200 UT on 27 December 1997) selected in this study was previously presented by Sutcliffe and Lyons [2002, hereinafter referred to as SL02]. In that study the authors showed several PBI-associated Pi2 bursts to occur simultaneously at high (magnetic latitude = 71°) and low (42°) latitudes under an extremely quiet geomagnetic condition (*Kp* = 0+ for 1800–2100 UT and 0 for 2100–2400 UT). The authors focused on the occurrence of Pi2 bursts associated with the plasma variations in the plasma sheet, but they did not include an examination of the wave characteristics in their study. We examine in detail the PBI-associated Pi2 (hereinafter referred to as PBI-Pi2) pulsations using ground-based data from latitudinally and longitudinally extended magnetometer network and data from the Polar spacecraft located on the duskside magnetosphere.

3.1. Overview of PBI-Pi2 Events

[11] The provisional auroral electrojet indices *AL* and *AU* and filtered *H*-component magnetometer data from Kvistaberg (KVI) (*L* ~3.3, local time ~UT +1.2 hours), which is one of SAMNET ground stations, are plotted in Figures 1a and 1b, respectively. In the KVI data we identify six major Pi2 bursts occurring at 1829 UT (event A), 1901 UT (event B), 1935 UT (event C), 2006 UT (event D), 2041 UT (event E), and 2115 UT (event F). The onsets of the bursts are marked by the vertical dotted lines. These are the same as the Pi2 bursts observed at the low-latitude Hermanus (HER, *L* ~1.9, local time ~UT +1.3 hours) station in SL02. During the interval 1800–2200 UT, the magnitudes of *AU* and $|AL|$ are less than 10 nT. Unlike substorm-associated Pi2 pulsations, there are no sudden decreases in *AL* accompanied by the Pi2 bursts. Note that the KVI data are filtered 4–10 mHz (100–250 s), which is the lower limit of the Pi2 frequency range. We will show below that dominant spectral peaks of the PBI-Pi2 pulsations are in the frequency range of 4–10 mHz.

[12] Figure 2 shows the unfiltered magnetic field data from selected IMAGE stations at magnetic latitude between ~65° and ~76°. This plot is the same as Figure 2 in SL02 but including the *Z* component. The vertical dashed lines indicate the onsets of the Pi2 bursts at KVI. The ground stations are ordered from the highest corrected geomagnetic latitude at the top to the lowest at the bottom. The IMAGE stations were in the local magnetic midnight at ~2100 UT. From the IMAGE magnetometer data, it is inferred that the westward electrojet was centered at a latitude between Hopen Island (HOP) and Bear Island (BJN) based on the latitude at which the perturbation in the *X* component is a maximum and the *Z* component changes sign. The ampli-

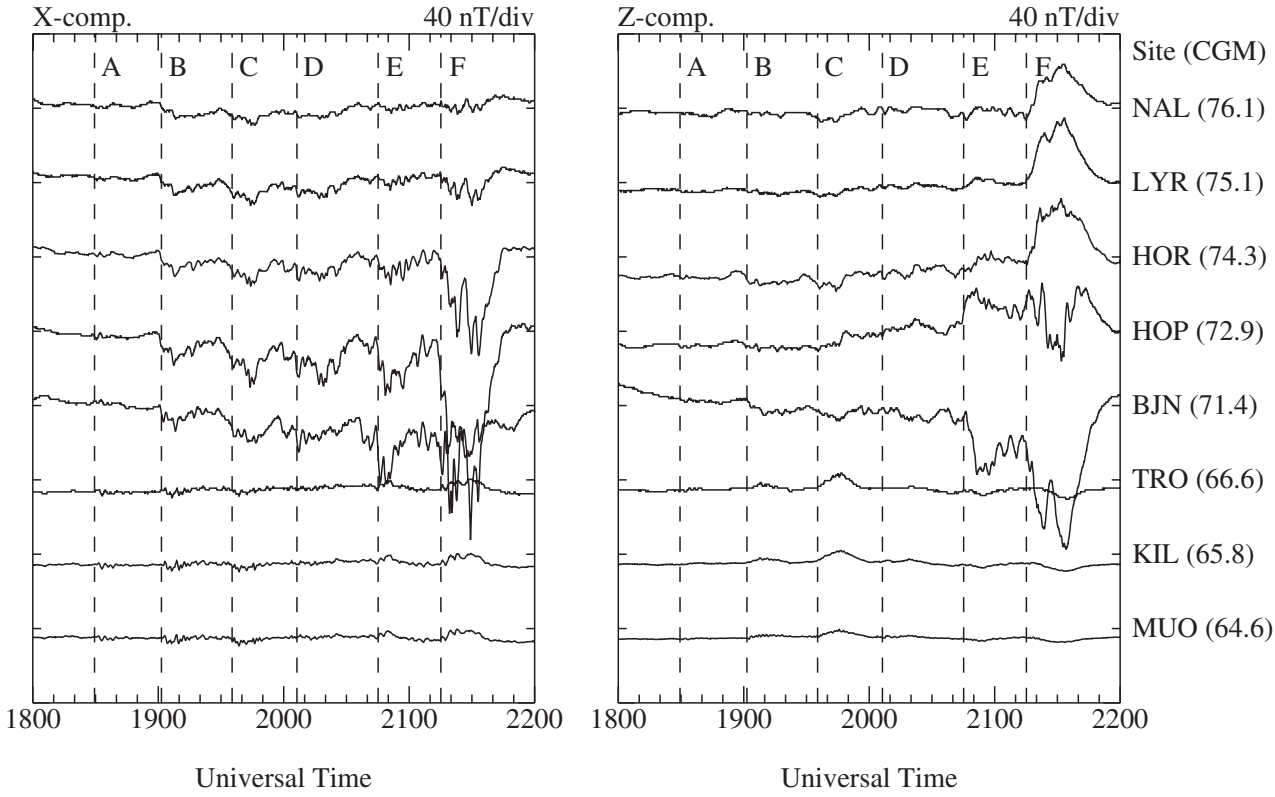

Figure 2. *X* and *Z* component magnetic field data at International Monitor for Auroral Geomagnetic Effects (IMAGE) stations.

tudes of the fluctuations in the *X* and *Z* components at HOP and BJN were much larger for the interval from 2100 to 2200 UT than that from 1900 to 2100 UT. This indicates that the electrojet intensification was localized around the midnight. Although several negative excursions in the *X* component occurred at magnetic latitudes above 71° look like negative bays, their magnitudes were significantly less than for typical substorms. There were no negative excursions of the *X* component at latitudes below 67°. These observations suggest that the Pi2 pulsations are associated with PBIs but not with substorms, as noticed in SL02. Events B to F occurred during negative excursions of the *X* component at the higher-latitude stations (Ny lesund (NAL) to BJN), while event A was not accompanied by the negative perturbation.

[13] The midlatitude, low-latitude, and dip equator *H* component data filtered by removing 600-s running averages are plotted in Figure 3. The magnetic latitude, magnetic local time at 2000 UT, and *L* value are plotted to the right and left of each magnetic trace. Oulu (OUL), York (YOR), and HER are located on similar local time meridians, in the premidnight sector during the interval, 1800–2200 UT. KAK and Ancon (ANC) were located in the postmidnight and afternoon dip equator, respectively, for the 4-hour interval. The PBI-Pi2 bursts are clearly seen at OUL, YOR, and HER in the premidnight sector. Their amplitude at HER is smaller that that at OUL and YOR by a factor of ~2. Although we can identify the magnetic field perturbations during events A to C at KAK in the postmidnight sector starting at the onset times of the Pi2 bursts in the premidnight sector, the PBI-Pi2 pulsations at KAK are not as clear as at the stations in the premidnight. KAK was located near the dawnside (0500–0600 MLT) during the intervals of events D to F and had no perturbations similar to those occurring at HER, YOR, and OUL. These indicate that the region of the pulsations was not extended to dawn. The PBI-Pi2 pulsations at the afternoon dip equator (ANC) are quite similar to those in the premidnight sector. Their amplitude was strongly enhanced and comparable to that at OUL. This enhancement at the dayside equator is similar to the substorm-associated Pi2 pulsations [*Shinohara et al.*, 1997, 1998].

[14] Figures 4a and 4b show the band-integrated (3–25 mHz) amplitude A_{Pi2} and frequency with a well-defined spectral peak in a moving 10-min time window, respectively, using the autoregressive spectral analysis technique for the *H*-component ground station data in Figure 3. Detailed descriptions of this technique are given by *Takahashi et al.* [2002a]. The vertical dashed lines are the same as in Figure 1. Repetitive enhancements of the band-integrated amplitude, each of which is due to a PBI-Pi2 burst, are clearly seen at the longitudinally and latitudinally separated five ground stations. The A_{Pi2} variations are almost identical among the stations. As shown in SL02 (see Figure 4 in their study), the PBI-Pi2 bursts exhibit an excellent correlation with energetic particle enhancement in the plasma sheet. The particle enhancements and Pi2s are consequence of the large-scale processes that give rise to plasma sheet flow bursts and associated plasma sheet magnetic field variations.

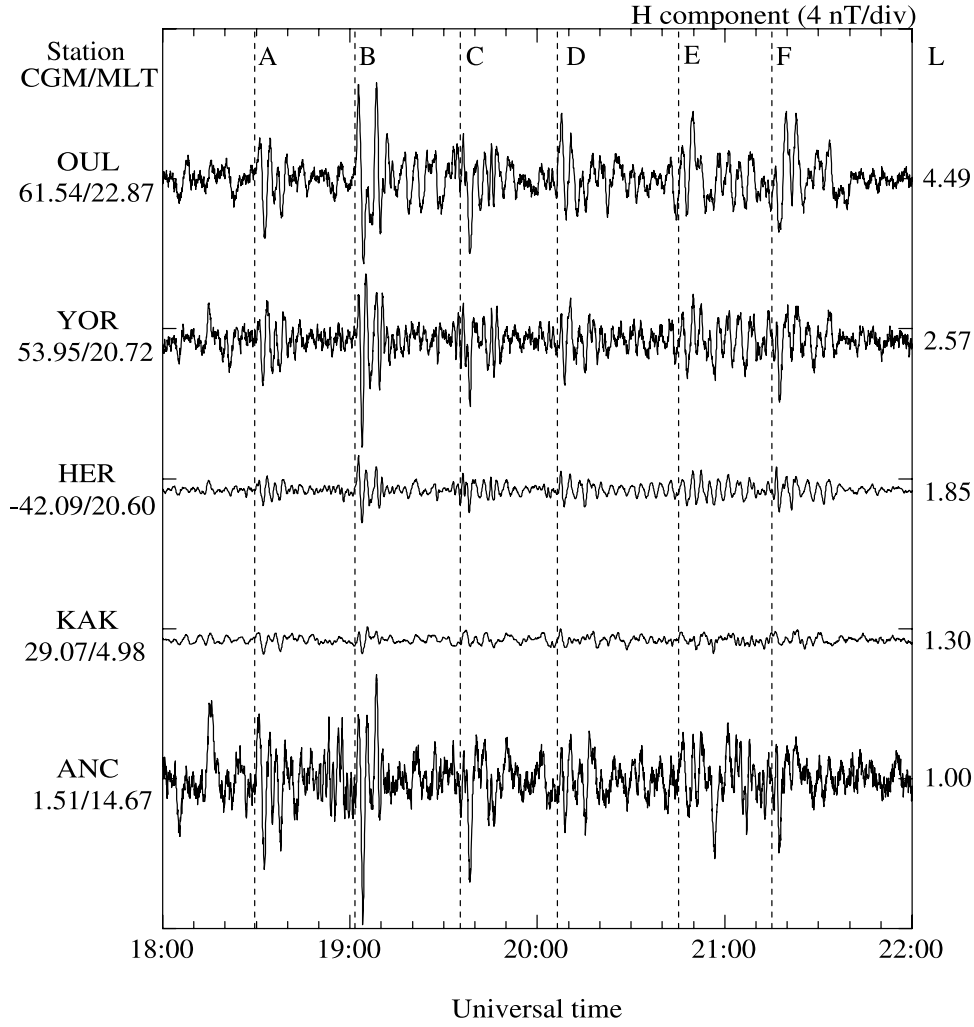

Figure 3. High-pass-filtered time series of ground data. The filtering was done by removing running 600-s average from the 5-s data.

[15] Frequencies of spectral peaks in the bandwidth, 3–25 mHz, are plotted in Figure 4b. The arrows indicate around the frequencies corresponding to the amplitude peaks for events A to F. The peak frequencies are distributed between 4 and 10 mHz. During events A and B, the frequency at YOR was slightly higher than that at OUL. By contrast, events C and E show identical frequencies at YOR and OUL. Low-latitude KAK station in the postmidnight observed lower frequencies than at HER and YOR in the premidnight for events A and D. The frequency peaks at ANC are slightly different from those at other stations except for event B. From the variability of the frequency along the latitudes in the same time period, we suggest that the PBI-Pi2 perturbations observed in the middle/low latitudes are not dominated by only one mode structure such as a fast mode wave trapped in the plasmasphere [e.g., *Takahashi et al.*, 2001], which is mostly favored for a model of substorm-Pi2 pulsations in the inner magnetosphere or at middle/low latitudes.

[16] We examine whether the PBI-Pi2 pulsations are directly related to the westward current centered near at HOP (CGM = 73°). Figure 5a shows the raw and 10-min running averages of the *X*-component at HOP and the bandpass filtered (4–10 mHz) *H* component at KVI (CGM = 56°). HOP and KVI are located at similar local times 2378 MLT and 2213 MLT at 2200 UT, respectively. As mentioned in Figure 2, the HOP data are characterized by a series of negative perturbations due to enhancements of the westward electrojet, which are associated with energetic particle flux enhancements within the plasma sheet. From HOP and KVI data, we confirm that the PBI-Pi2 bursts and the decrease in *X* at HOP are highly correlated except for event A, which may be due to the fact that the event was observed away from midnight. For events B to F the onset times of the bursts and the decrease in *X* are different. That is, the Pi2 bursts are enhanced ~2–6 min after the *X* decrease. Such a timing difference between high-latitude *X* component decrease and lower-latitude Pi2 onset is also reported by *Kepko et al.* [2004]. The PBI-Pi2 bursts disappear while the HOP *X* component increases. These observations imply that the electrojet is not the initial cause of the PBI-Pi2 oscillations at midlatitude but that the enhancements of the PBI-Pi2 bursts are modulated from the intensification of the electrojet current.

[17] It is believed that the ionospheric currents are fed by field-aligned currents, which is connected to the plasma sheet and directed downward in the postmidnight sector and upward in the premidnight sector. That is, if the currents

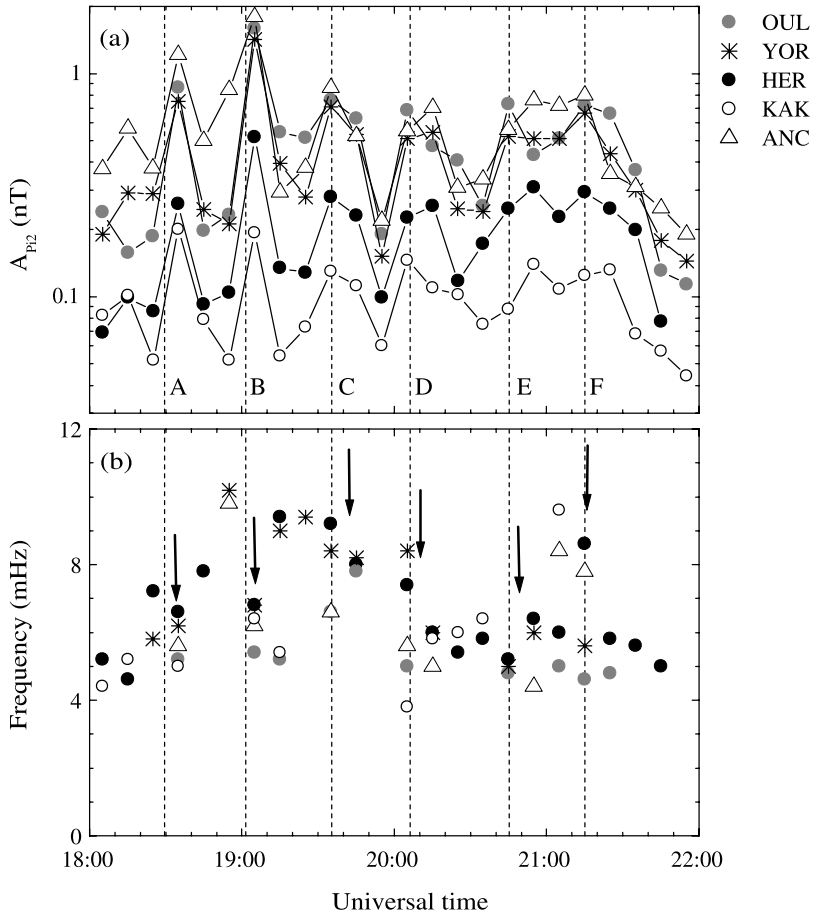

Figure 4. (a) Band-integrated (3–25 mHz) amplitude A_{Pi2} and (b) frequencies at the spectral peaks at midlatitude, low-latitude, and equatorial ground stations.

flow on the wedge-shaped circuit, as expected during substorm onsets, the positive (negative) *D* perturbations in Figure 5b can be interpreted as that OUL and YOR in the premidnight (KAK in the postmidnight) was located west (east) of the center of the current wedge [*Clauer and McPherron*, 1974]. The *H* (*D*) component at YOR exhibits the negative (positive) perturbations for events A, B, C, and D, indicating that the station was located west of the upward field-aligned current part of the wedge. OUL showed the strong positive *D* perturbation for events B and C, but a baseline change in *H* was not clear as much as at YOR. This indicates that OUL was close to the upward field-aligned current. The positive perturbations in *H* and *D* at OUL and YOR for event F imply that both stations were inside the current wedge.

3.2. Latitudinal Wave Characteristics

[18] Both latitudinal and longitudinal structures are important in determining the cause of the Pi2 pulsations. We examine the latitudinal structure first. Figure 6 shows the data for events A and B from nine stations located in the premidnight sector (1900–2300 MLT). The ground data have been filtered by removing 600-s running averages from *H* and *D* components. Selected stations at higher latitudes and lower latitudes are grouped into Figures 6a and 6b, respectively. The vertical dashed lines indicate the peaks of the perturbations at YOR.

[19] During event A, the oscillations in the *H* component at lower latitudes (Figure 6b) started simultaneously at around 1830 UT, but after one cycle a considerable phase lag appeared among the stations. The phase lag was smaller between YOR and KVI than between YOR and OUL. The phase lag increases gradually with increasing latitudes. This indicates that the perturbations at OUL, KVI, and YOR are excited by a common source and then they showed latitude-dependent oscillations (i.e., slightly longer period at higher latitude). However, the *D* component at OUL and KVI has no phase delay with the *H* component at YOR. That is, the oscillations in D at OUL and KVI and in H at YOR have nearly identical waveform. The power spectrum of the perturbations in *H* and *D* at OUL and YOR for event A is plotted in Figure 7. The spectrum was obtained using the maximum entropy method [*Ulrich and Bishop*, 1975] with the number of the poles of six. The OUL *D* and YOR *H* and *D* have an identical spectral peak at 6 mHz, but OUL *H* has a spectral peak at 5 mHz. This suggests that the generation mechanisms of the perturbations in *H* and *D* at OUL are different. The amplitude at HER is smaller than that at SAMNET by a factor of ~2. The *D* and *H* components at HER oscillate out of phase. The *D* at HER in the southern hemisphere also oscillates out of phase with the *D* at OUL and KVI in the northern hemisphere. This signature would be expected when a motion of field lines is symmetric with respect to the magnetic equator. The

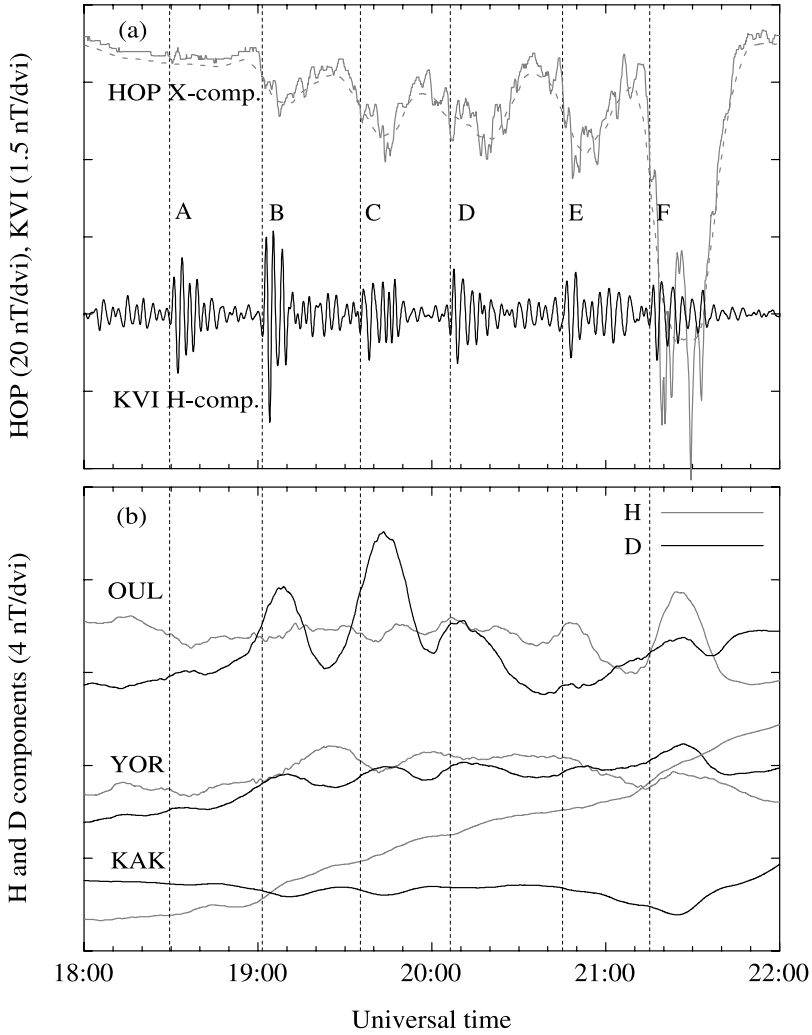

Figure 5. (a) Raw (gray solid line) and 10-min running averages (gray dashed line) of the *X* component at Hopen Island (HOP) and bandpass filtered (4–10 mHz) *H* component at KVI. (b) 10-min running averages from *H* and *D* components at middle/low latitudes.

oscillations in the *H* component at YOR and HER show nearly identical waveforms without a phase delay.

[20] A similar feature appears in the first two peaks of event B at the SAMNET stations. However, there is no phase delay for the third peak of event B, and its amplitude suddenly increased at OUL. This suggests that the field perturbations of event B were not due to a single source. It is obvious that the pulsation's period in *H* increases with increasing latitude from 51° to 62° for the intervals, 1840–1900 UT and 1910–1930 UT. That is, the period is longest at OUL and shortest at YOR. On the basis of these observations, we suggest that events A and B at the middle/low latitudes in the premidnight sector are attributed to latitudinally localized Alfvén waves. At KVI and YOR, the pulsations in the *D* component are much weaker than those in the *H* component, whereas the amplitude of the *D* component oscillation at OUL is comparable to that in *H*.

[21] The oscillations in the *H* and *D* components at Muonio (MUO) are similar to those at OUL (note different amplitude scale). For event A the *H* perturbations at BJN and NAL are roughly out of phase with *H* at MUO. The negative peak in *H* at HOP was earlier than that at higher (Hornsund (HOR), NLA) and lower (BJN) latitudes. Event B also shows a similar signature. The amplitude of the perturbations was largest around HOP for events A and B. These observations indicate that the source of the perturbations at high latitude is located near HOP and that the source moves higher and lower latitudes. Although the negative perturbations at the high latitudes appear to correspond to the positive perturbations at the lower latitudes, the generation mechanism at the middle/low latitudes may be different from that at high latitudes because there is no phase delay between OUL and HER at the first and third peaks of event B.

[22] Figure 8 shows the time series plot of event E using the same format as Figure 6. The SAMNET/IMAGE stations and HER were located in ~2150–0060 MLT. Unlike event A, the *H* component of event E has no apparent phase delay from OUL ($L \sim 4.5$) to HER ($L \sim 1.9$). The phase signature of event F (not shown) is similar to event E. The *H* and *D* components at OUL are roughly out of phase but in phase at YOR. Large fluctuations in the *H* and *D* components were observed at BJN and HOP. Their waveform and period differ from those at lower and higher latitudes. There are quasi-periodic perturbations at NAR

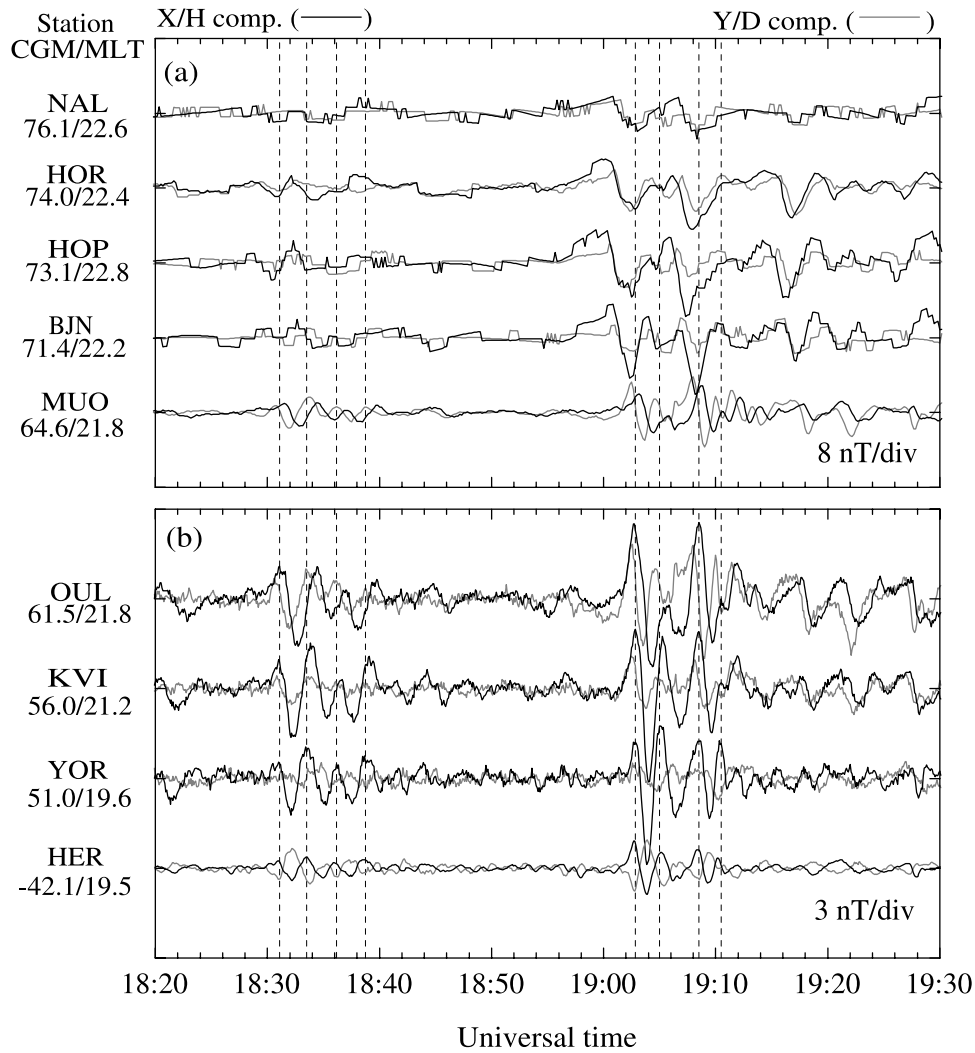

Figure 6. High-pass-filtered time series of selected (a) IMAGE stations and (b) Sub-Auroral Magnetometer Network (SAMNET)/Hermanus (HER) stations. The step-like variations at Ny lesund (NAL), HOP, and Bear Island (BJN) are due to a magnetic resolution of ~1 nT. The filtering was done by removing running 600-s average from the 5-s data. The vertical dashed lines indicate the peak perturbations at York (YOR).

and HOR. However, their period also differs from that at the SAMNET/HER stations.

[23] The interstation coherence and cross phase of events E and F were examined using the technique described by *Takahashi et al.* [2001] and the results are plotted in Figure 9. The solid (open) circles indicate event E (F). The coherence between YOR and other stations was calculated at the dominant frequency, 5 mHz (4.4 mHz) for event E (F). Figure 9b shows the amplitude ratio of the *H* component normalized to the value at YOR. The normalized amplitude and cross phase are plotted when the coherence was more than 0.8. High coherence occurs at MLAT < 65° ($L < 5.6$) with a cross phase of ~0°. The normalized amplitude increases with increasing latitude. The spectral peak at higher latitudes (MLAT >65°) occurs at lower frequency, as expected from Figure 8. As a consequence, coherence was low, implying that the source of the perturbations at high latitudes and at middle/low latitudes is different.

[24] Figure 10 shows the ground magnetic field data for event C. Although the magnetic perturbations at SAMNET/HER have irregular amplitude and period, the waveforms of the *H* perturbations from MUO to HER are nearly identical. The *H*-component data at high latitudes from BJN to NAL show also irregular form and some perturbations look like to oscillate out of phase with the lower-latitude data.

3.3. Longitudinal Wave Characteristics

[25] We examine the longitudinal properties of the Pi2 pulsations using Figures 11 and 12. Figure 11 shows the *H* component of CPMN and YOR data for events E and F. The *H*-component oscillations at the afternoon dip equator are nearly identical to those at YOR and exhibit no phase delay. Their amplitude is comparable to the perturbations at YOR. Similar *H* perturbations are observed at the postmidnight low-latitude stations at Yamakawa (YMK), Lunpin (LNP), and Muntinlupa (MUT) with much smaller amplitude but not at Tixie (TIK) and Magadan (MGD). The perturbations at Popov Island (PPI) were not clear as much as those at YOR. These observations suggest that

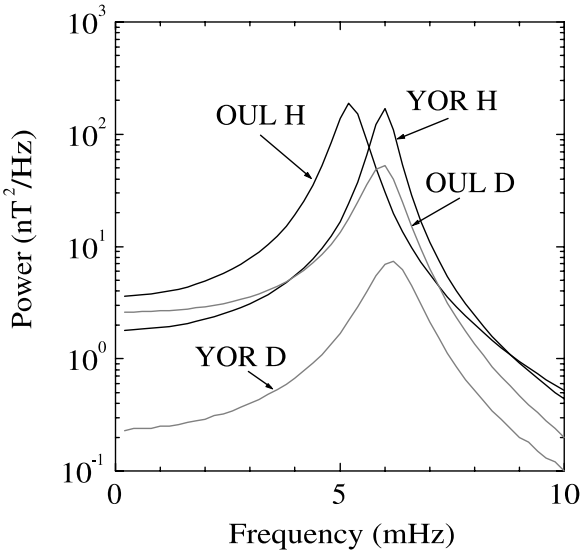

Figure 7. Maximum entropy method spectrum of the *H* and *D* components at Oulu (OUL) and YOR for event A.

the PBI-Pi2 pulsations were localized to latitudes lower than ~65° and to local time earlier than ~0500 MLT.

[26] The pulsations observed in the postmidnight sector during events A and B are plotted in Figure 12a. Unlike in Figure 11, MGD (0410 MLT) observed similar *H* perturbations to those at lower latitudes in the postmidnight, which are nearly identical to the perturbations at YOR, with a phase delay of ~180°. The amplitude of the perturbations at ANC is larger that that at YOR. Following the vertical dashed lines in Figure 12a, we find that the second peaks of events A and B at YOR lead those at ANC. As shown in Figure 6, such a signature occurred at higher latitudes (KVI and OUL). To emphasize this point, we have plotted the *H*-component data from the SAMNET stations with the ANC data in Figure 12b. Although the dominant perturbations at ANC are quite similar to those at SAMNET stations, the dayside dip equator perturbations are more closely related to the perturbations at higher latitudes than at YOR in terms of a phase variation.

3.4. Comparison With Polar Spacecraft Data

[27] Figure 13 illustrates the Polar orbit in the SM (solar magnetic) coordinates for the 2-hour interval,

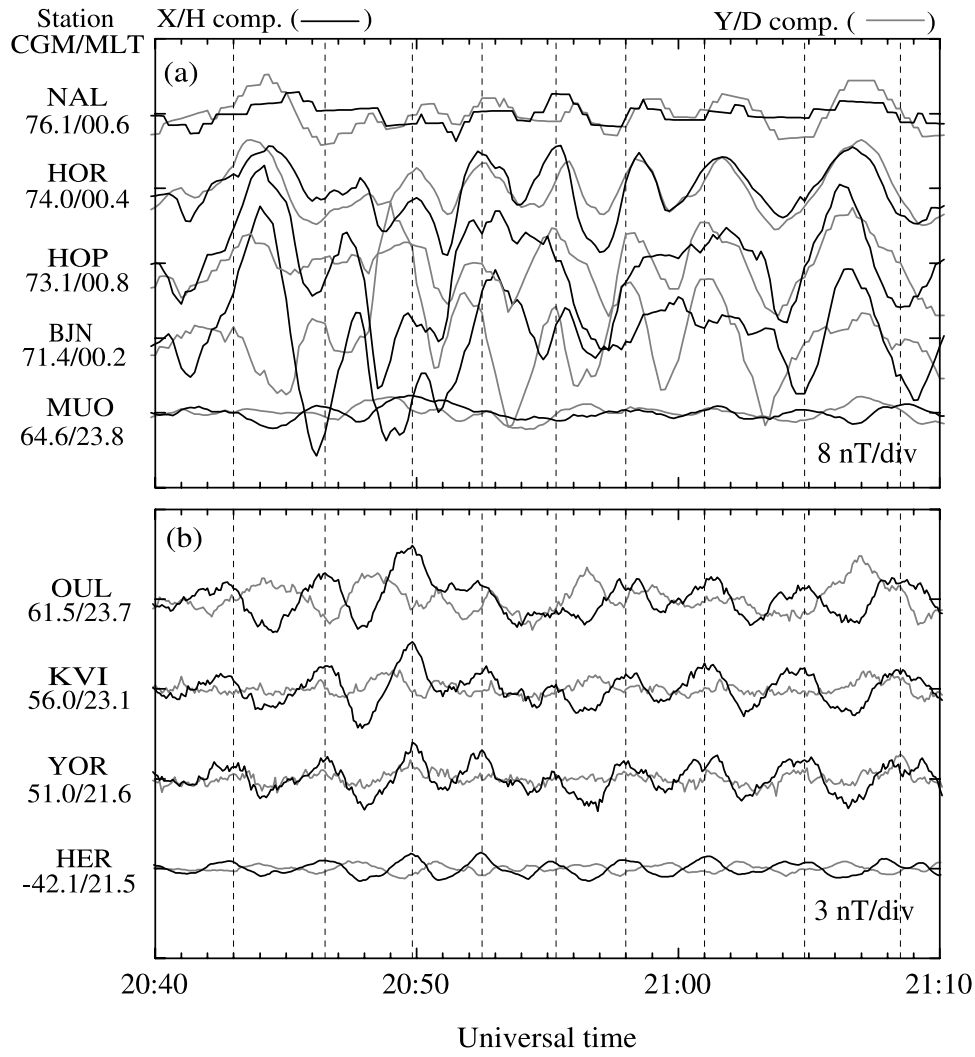

Figure 8. Same as Figure 6, but for the interval of event E.

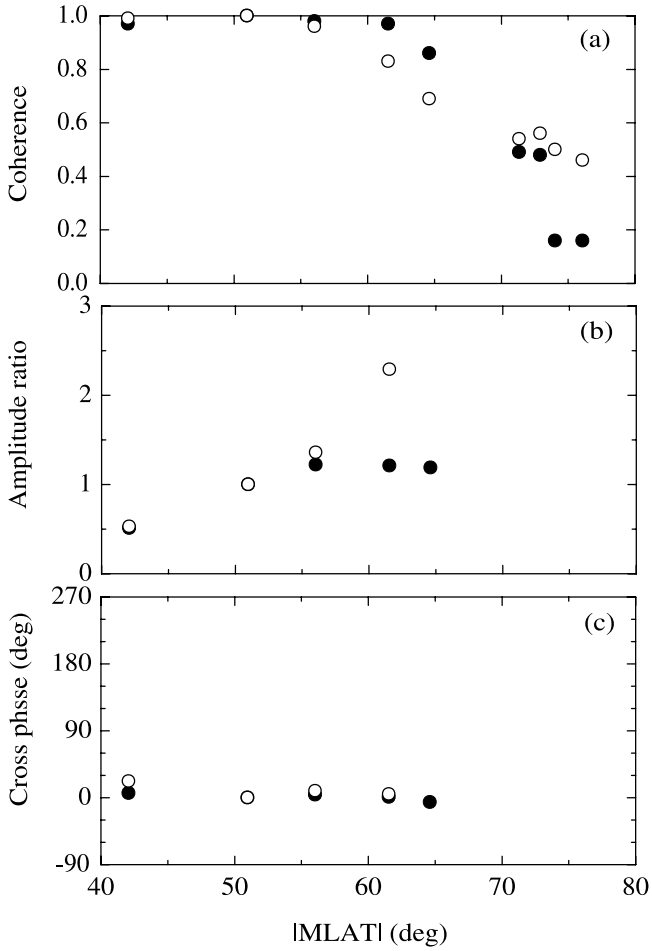

Figure 9. Interstation (a) coherence, (b) amplitude ratio, which is defined as the square root of other station H to YOR H power ratio, and (c) cross phase for the H component of events E (solid circles) and F (open circles).

1800–2200 UT. The satellite locations are plotted with the solid lines, marked every 1 hour by the solid circles. The orbital plane of the Polar spacecraft was close to the dawn-dusk meridian. During the interval from 1900 to 2200 UT, Polar crossed L shells between ~3 and ~15 in the 1800–1900 MLT sector, moving from 2.1 to 6.4 R_E geocentric distance.

[28] Figure 14 shows the plasma density estimated from the spacecraft potential data [*Scudder et al.*, 2000] and the location of Polar as a function of universal time, using the magnetic shell parameter L. There are spiky variations and the large dip in the plasma density between 1918 and 1947 UT. This is due to instrumental errors (available at http://lepefi.gsfc.nasa.gov/~polarefi), occurring in the plasmasphere near perigee (~1.8 R_E). The plasma density did not have a simple radial structure. Polar observed quasi-periodic density variations in the range of ~40–300 cm^{-3} between $L \sim 5$ and $L \sim 7$. Since a typical plasmapause crossing is characterized by a density decrease from above 100 cm^{-3} to below 10 cm^{-3}, we do not attribute such variations to plasmapause crossings. They could be considered as a temporal or spatial density change in the plasmasphere.

[29] The density decreased from 100 cm^{-3} at ~2050 UT to below 10 cm^{-3} ~2125 UT, corresponding to an L range from 7 to 10. We suggest that a plasmapause was located somewhere beyond L ~7. Such a plasmapause's location can be expected in the duskside region during a quiet geomagnetic condition, $Kp \leq 1$ [*Chappell*, 1972]. At small radial distance the despun magnetic and electric field data are contaminated by artificial oscillations, and at L >10 very irregular field perturbations were observed. Clean segment of the field data from Polar was the interval from ~2030 to ~2130 UT.

[30] Figure 15a shows the time series of compressional magnetic field (b_{zMFA}), azimuthal magnetic field (b_{yMFA}), and radial electric field (E_{xy}) components for event E. The E_{xy} and the smoothed traces in b_{zMFA} and b_{yMFA} are filtered in the frequency band 2–10 mHz. The perturbations in B_{56} are nearly identical to those in $-b_{yMFA}$ (not shown here). It is clear that the E_{xy} oscillated in phase with b_{yMFA} at ~34°–37° magnetic latitude, indicating that the Alfvén mode is propagating. Such a propagating Alfvén mode at high magnetic latitudes in the plasmasphere has been reported by *Osaki et al.* [1998]. The compressional (b_{zMFA}) and azimuthal (b_{yMFA}) components have different period.

[31] Oscillations in space and on the ground for event E are compared in Figure 15b. The figure includes the H component at OUL ($L \sim 4.5$) and YOR ($L \sim 2.6$), filtered by removing 10-min running average, and the b_{yMFA} component at Polar, filtered in the frequency band 2–10 mHz. Note that b_{yMFA} in Figure 15b is shifted to the left by 50 s in order to match the ground perturbations. The ground H component has a great similarity with the perturbation in b_{yMFA}. This implies that the ground perturbations are associated with the transverse mode in space rather than the compressional mode.

4. Discussion

[32] Previous observations on the ground at middle/low latitudes [e.g., *Stuart*, 1974; *Yeoman and Orr*, 1989; *Lin et al.*, 1991] and in space in the inner ($L < 5$) magnetosphere [*Takahashi et al.*, 1995] showed that the plasmaspheric cavity mode (i.e., fast-mode waves trapped in the plasmasphere) is a promising mechanism for Pi2 pulsations. The frequency of the plasmaspheric cavity mode depends on the radial distance of the plasmapause [*Takahashi et al.*, 2003]. We suggested from the Polar data that the plasmapause was located at $L \geq 7$. For this distance, the cavity mode frequency is expected to be less than 6.5 mHz, assuming simple box geometry and a constant Alfvén velocity, 500 km/s [*Takahashi et al.*, 2003]. The peak frequencies of events A–F in our study are within the band of ~4–10 mHz. Thus our PBI-Pi2 events observed at middle/low latitudes could be the plasmaspheric cavity mode in terms of frequency.

[33] However, the latitude-dependence of the frequency during events A and B argues against the plasmaspheric cavity mode because an identical frequency at latitudinally extended stations inside the plasmasphere is expected. The amplitude maxima in the H/X component near the location, the magnetic latitude between 65° and 71°, of the phase reversal during events A and B (see Figure 6) in the

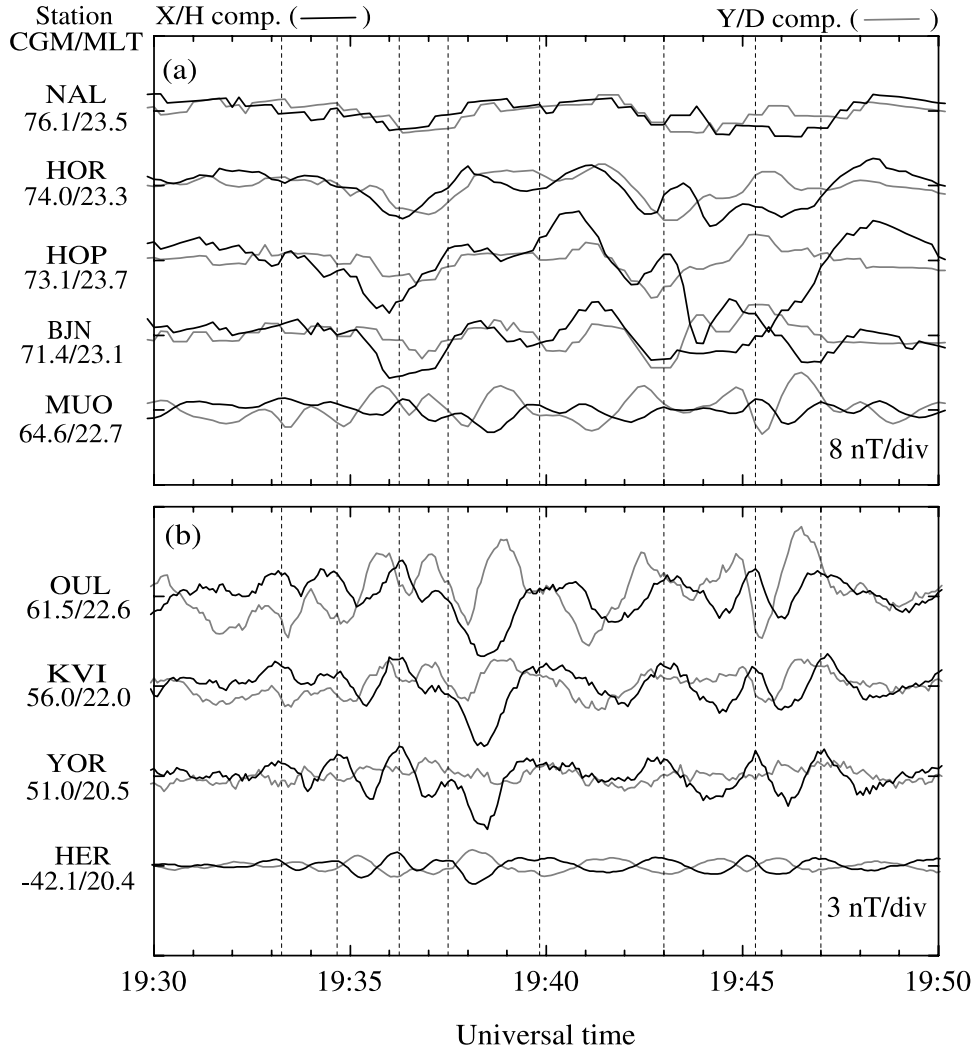

Figure 10. Same as Figure 6, but for the interval of event C.

premidnight sector would be attributed to that the field line is connected to the source region or to the region of strong mode conversion [*Chen and Hasegawa*, 1974; *Southwood*, 1974]. The amplitude variation with latitude near a phase-jump location is opposite to that expected from the cavity mode model of Pi2 [*Takahashi et al.*, 1995] if compressional oscillation maps to the northward (H/X) component on the ground without phase shift [e.g., *Takahashi et al.*, 1999]. In the postmidnight sector the phase reversal occurred around 54° magnetic latitude (see Figure 12). This would be interpreted as that the location of the mode conversion in the premidnight and postmidnight is different.

[34] Recently, *Kepko and Kivelson* [1999] proposed that the midlatitude/low-latitude Pi2 pulsations can be driven by fast-mode pulses generated as periodic bursty bulk flows brake in the near-Earth magnetotail. *Kepko et al.* [2001] suggested that Pi2 pulsations have different features at different locations along latitude and longitude. According to their model, current perpendicular to the magnetic field and directed dawnward is generated by the inertia effect of flow braking. The perpendicular current is diverted into the field-aligned currents that flow on a wedge-shaped circuit connected to the ionosphere. The current system decays as the flow disappears but it intensifies again when the next flow burst arrives. Although the magnetotail observations by the Geotail spacecraft missed the fast earthward flow bursts during the interval in our study because the spacecraft was far away from the Sun-Earth line, SL02 showed that the PBI-Pi2 bursts are strongly correlated with external source (i.e., energetic particle enhancements). Therefore our PBI-Pi2 events may have source dependent signatures. The period and duration of the pulsation may be determined at the source. Event C showed very irregular waveform and period (see Figure 10) even though it occurred during a period of extremely quiet geomagnetic condition.

[35] From the time-modulated current model [*Kepko et al.*, 2001], three effects can be expected: (1) The region of perpendicular current acts as a source of propagating fast mode pulses. The pulse propagates earthward across the equatorial magnetic field and produces equatorial Pi2 pulsations on the ground. (2) Field-aligned current produces additional ground perturbations on east-west component at midlatitude. (3) The fast-mode pulses propagating on the flank side forces the field lines to oscillate azimuthally, resulting in Alfvénic perturbations in the flankside magnetosphere, and such Alfvénic perturbations are observed in the northward (H/X) component on the ground.

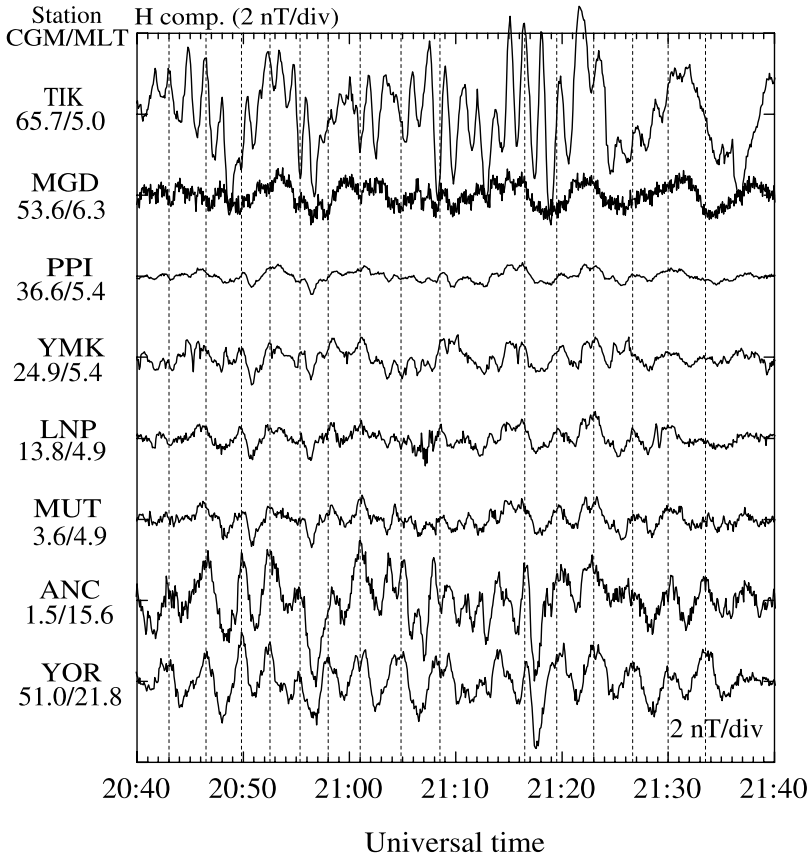

Figure 11. High-pass-filtered time series of selected CPMN/YOR stations.

[36] We showed that event A has a spectral peak at 5 mHz in the *H* component at OUL but a spectral peak at 6 mHz in OUL *D* and YOR *H*/*D* (see Figure 7). Since YOR and OUL were outside the expected current wedge in the premidnight sector (1910–2130 MLT) for event A, the initial positive *H* perturbations at midlatitudes exclude the field-aligned current model. The *H*-component oscillation at OUL may be categorized as frankside Pi2 associated with Alfvénic signature discussed by *Kepko and Kivelson* [1999] and *Kepko et al.* [2001] (see their Figure 15).

[37] According to a statistical study of fundamental standing Alfvén waves [*Takahashi et al.*, 2002b], the 5-mHz fundamental standing Alfvén waves are expected at $L \sim 8-10$ in the duskside. Therefore the 5-mHz oscillation is far from the fundamental standing Alfvén wave frequency at OUL ($L \sim 4.5$). That is, it is not clear whether the 5-mHz oscillation on the ground is caused by Alfvén resonance at $L \sim 4.5$. We suggest that the *H*-component oscillations at OUL would result from transient Alfvénic perturbations excited by a series of compressional pulses, which may be associated with braking of oscillatory earthward flows.

[38] The interstation coherence and cross-phase analysis of the *H* component of events E and F showed that the high coherence occurs at middle/low latitudes (MLAT $< 65°$) without a phase delay and that the amplitude of high-coherence event increases with increasing latitude (Figure 9). The large amplitude at higher latitudes indicates that the source of the perturbations is at higher latitudes. Such a source would be considered as field-aligned current associated with perpendicular current [*Kepko et al.*, 2001]. Event F was inside of the current wedge as mentioned above (Figure 5). Although the background bay signature was not clear to identify ground locations with respect to the current wedge for event E, the out of phase (in phase) *H* and *D* components at OUL (YOR) would be expected from the field-aligned current model if both stations are inside the current wedge and YOR (OUL) is close to the western (eastern) field-aligned current part. Note that OUL was located ~2 hours east of YOR.

[39] The PBI-Pi2 pulsations at midlatitude were not seen in the dawnside but occurred in the duskside. This longitudinal asymmetry may indicate a localization of the source disturbance. If the PBI-Pi2 events are associated with the earthward flow bursts in the magnetotail, the flow channel is skewed to the premidnight region [*Angelopoulos et al.*, 1996].

[40] Polar in the duskside at ~34°–37° magnetic latitude observed compressional and transverse oscillations during event E. We have compared the oscillations in space and *H* on the ground and find that the ground Pi2 pulsations have nearly the same period as the transverse oscillations in space. Previous ground-satellite observations near midnight [e.g., *Takahashi et al.*, 1995; *Keiling et al.*, 2001] and near dawn [*Nosé et al.*, 2003] showed that ground Pi2 pulsations are correlated with the compressional oscillations near the magnetic equator. *Osaki et al.* [1998] reported that no Pi2 pulsations was detected in the compressional component at ~30°–40° magnetic latitude near midnight and that the period of the ground Pi2 pulsations was nearly identical to that in the transverse component.

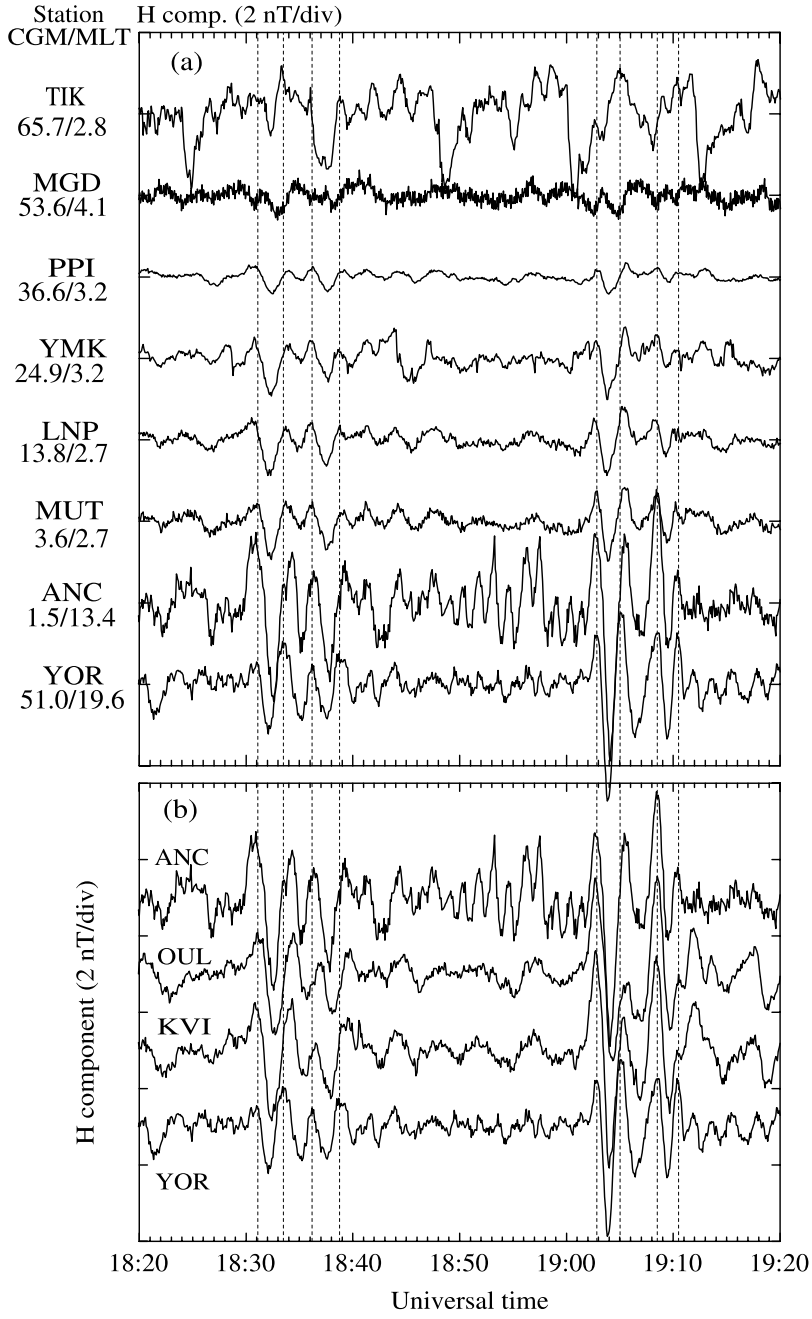

Figure 12. (a) Same as Figure 11, but for the interval of events A and B. (b) Comparison of the *H*-component perturbations at the dayside dip equator and the selected nightside midlatitudes.

From these observations we suggest that the spacecraft signatures depend on the local times as well as magnetic latitude. As shown in Figure 15, *L* dependence of frequency in the transverse component was not clear. Therefore the transverse perturbations near dusk may be transient Alfvénic mode associated with the fast mode pulses propagating on the flank side, which are caused by flow braking [*Kepko et al.*, 2001].

[41] We showed that the PBI-Pi2 bursts at middle/low latitudes are correlated with the negative bay disturbances (i.e., PBI) at current source region (magnetic latitude = $\sim$73°) but that the initial perturbations of the Pi2 pulsations do not match with the onset time of the bay disturbance. That is, the Pi2 bursts are enhanced $\sim$2–6 min after the negative bay. This indicates that the source of the negative bay is located further away from the Earth in the tail than the source region of the PBI-Pi2 pulsations.

5. Conclusions

[42] We have examined the PBI-Pi2 pulsations that occurred during the absence of substorms and during ground state geomagnetic conditions (*Kp* = 0). As noticed in SL02, the PBI-Pi2 bursts occurred periodically every $\sim$30 min and were correlated with bay-like disturbances at high latitudes, associated with energetic particle enhancements in the plasma sheet. The bay-like disturbances are considered as a result of westward electrojet currents flow-

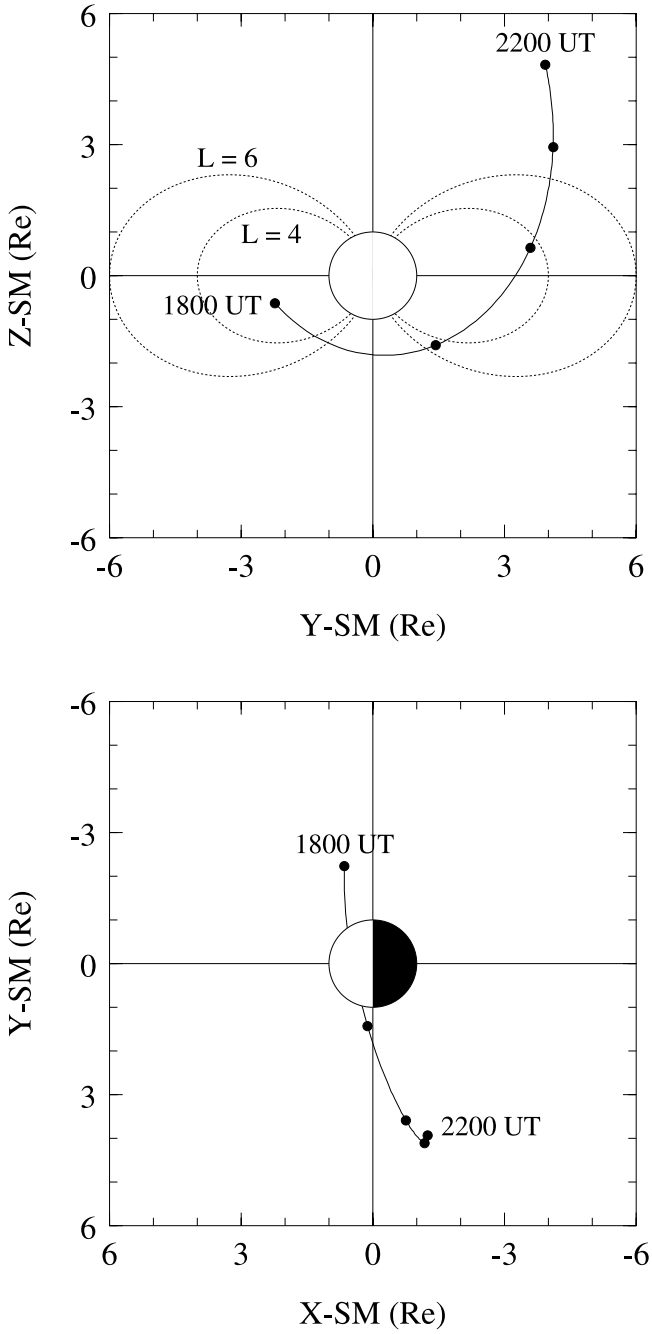

Figure 13. Orbit of the Polar spacecraft for the interval of 1800–2200 UT on 27 December 1997. The orbit is projected onto the solar magnetic (top) *y-z* and (bottom) *x-y* plane.

ing around 73° magnetic latitude. Although the PBI-Pi2 bursts are correlated with the negative disturbances, the initial cause of the PBI-Pi2 pulsations is not the westward current. We observed that the PBI-Pi2 pulsations at middle/low latitudes have different features at different local times, that is, Alfvénic signatures near the duskside and no phase delay near the midnight with latitudes. These observations could be interpreted by the model presented by *Kepko et al.* [2001]. According to their model, the period and duration of the Pi2 pulsation are determined at a source region, where fast earthward flows brake. The PBI-Pi2 pulsations in our

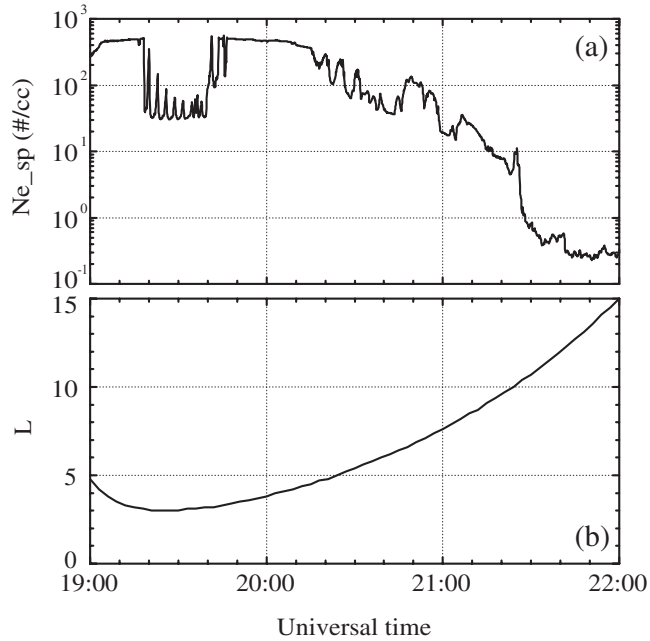

Figure 14. (a) Plasma density estimated from the spacecraft potential data. (b) Dipole shell parameter *L* for the interval of 1900–2200 UT.

study have an irregular period and amplitude even though during very quite geomagnetic condition. Our observations would be attributed to source dependent signature rather than plasmaspheric cavity mode. However, we need a direct

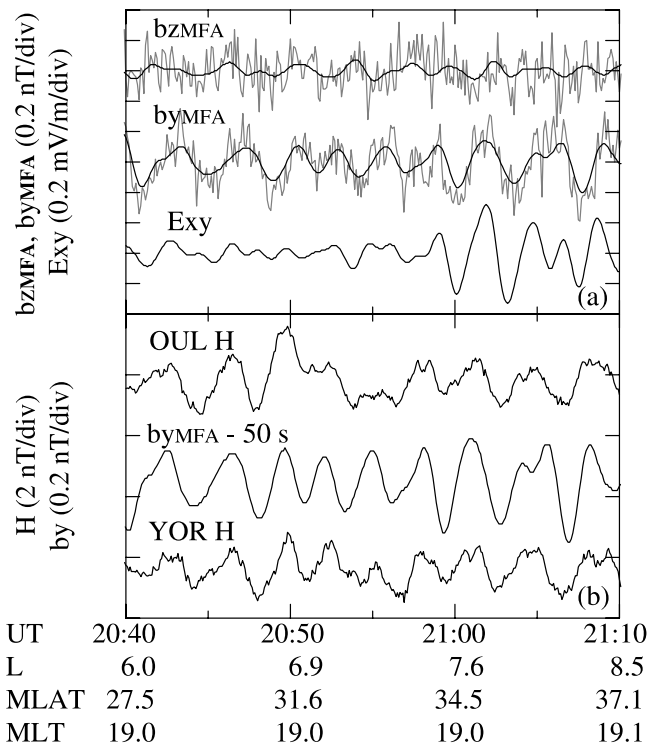

Figure 15. (a) b_{zMFA}, b_{yMFA}, and E_{xy} for event E. The smoothed traces in b_{zMFA} and b_{yMFA} and E_{xy} are filtered (2–10 mHz). (b) Comparison of the b_{yMFA} component at Polar and the *H*-component at OUL and YOR.

comparison between PBI-Pi2 pulsations and flow variations in the tail to make a conclusion which model is favored for the PBI-Pi2 pulsations. In the future we will attempt to do a statistical survey of PBI-Pi2 events with spacecraft observations in the tail.

[43] **Acknowledgments.** We thank the SAMNET team for magnetometer data. SAMNET is a PPARC National Facility operated by Lancaster University. We thank the institutes who maintain the IMAGE magnetometer array. We are grateful to C. T. Russell for the Polar magnetic field data and to F. S. Mozer for the Polar electric field data. We also thank CPMN magnetometer team. The ground Kakioka data and the provisional auroral electrojet indices were provided by the Kakioka Observatory. This work was supported by Korea Science and Engineering Foundation grant R14-2002-043-01000-0. Work at JHU/APL was supported by NASA under grant NAG5-13119.

[44] Arthur Richmond thanks Larry Kepko and Larry Lyons for their assistance in evaluating this paper.

References

Angelopoulos, V., et al. (1996), Multipoint analysis of a bursty bulk flow event on April 11, 1985, *J. Geophys. Res.*, *101*, 4967.

Chappell, C. R. (1972), Recent satellite measurements of the morphology and dynamics of the plasmasphere, *Rev. Geophys.*, *10*, 951.

Chen, L., and A. Hasegawa (1974), A theory of long-period magnetic pulsations, 1, Steady state excitation of field line resonance, *J. Geophys. Res.*, *79*, 1024.

Clauer, C. R., and R. L. McPherron (1974), Mapping the local time-universal time development of magnetospheric substorms using mid-latitude magnetic observations, *J. Geophys. Res.*, *79*, 2811.

Fukunishi, H. (1975), Polarization changes of geomagnetic Pi 2 pulsations associated with the plasmapause, *J. Geophys. Res.*, *80*, 98.

Harvey, P., et al. (1995), The electric field instrument on the Polar satellite, in *The Global Geospace Mission*, edited by C. T. Russell, p. 583, Springer, New York.

Keiling, A., J. R. Wygant, C. Cattell, K.-H. Kim, C. T. Russell, D. K. Milling, M. Temerin, F. S. Mozer, and C. A. Kletzing (2001), Pi2 pulsations observed with the Polar satellite and ground stations: Coupling of trapped and propagating fast mode waves to a midlatitude field line resonance, *J. Geophys. Res.*, *106*, 25,891.

Kepko, L., and M. Kivelson (1999), Generation of Pi2 pulsations and bursty bulk flows, *J. Geophys. Res.*, *104*, 25,021.

Kepko, L., M. Kivelson, and K. Yumoto (2001), Flow bursts, braking, and Pi2 pulsations, *J. Geophys. Res.*, *106*, 1903.

Kepko, L., M. G. Kivelson, R. L. McPherron, and H. E. Spence (2004), Relative timing of substorm onset phenomena, *J. Geophys. Res.*, *109*, A04203, doi:10.1029/2003JA010285.

Kim, K.-H., K. Takahashi, D.-H. Lee, N. Lin, and C. A. Cattell (2001), A comparison of Pi2 pulsations in the inner magnetosphere and magnetic pulsations at geosynchronous orbit, *J. Geophys. Res.*, *106*, 18,865.

Lin, C. A., L. C. Lee, and Y. J. Sun (1991), Observations of Pi 2 pulsations at a very low latitude (L = 1.06) station and magnetospheric cavity resonances, *J. Geophys. Res.*, *96*, 21,105.

Lühr, H., A. Aylward, S. C. Buchert, A. Pajunpää, K. Pajunpää, T. Holmboe, and S. M. Zalewski (1998), Westward moving dynamic substorm features observed with the IMAGE magnetometer network and other ground-based instruments, *Ann. Geophys.*, *16*, 425.

Lyons, L. R., T. Nagai, G. T. Blanchard, J. C. Samson, T. Yamamoto, T. Mukai, A. Nishida, and S. Kokubun (1999), Association between Geotail plasma flows and auroral poleward boundary intensifications observed by CANOPUS photometers, *J. Geophys. Res.*, *104*, 4485.

Nosé, M., et al. (2003), Multipoint observations of a Pi2 pulsation on morningside: The 20 September 1995 event, *J. Geophys. Res.*, *108*(A5), 1219, doi:10.1029/2002JA009747.

Olson, J. V., and G. Rostoker (1975), Pi2 pulsations and the auroral electrojet, *Planet. Space Sci.*, *23*, 1129.

Osaki, H., K. Takahashi, H. Fukunishi, T. Nagatsuma, H. Oya, A. Matsuoka, and D. K. Milling (1998), Pi 2 pulsations observed from the Akebono satellite in the plasmasphere, *J. Geophys. Res.*, *103*, 17,605.

Russell, C. T., et al. (1995), The GGS/Polar magnetic fields investigation, in *The Global Geospace Mission*, edited by C. T. Russell, p. 563, Springer, New York.

Saito, T. (1969), Geomagnetic pulsations, *Space Sci. Rev.*, *10*, 319.

Saito, T., and S. Matsushita (1968), Solar cycle effects on geomagnetic Pi 2 pulsations, *J. Geophys. Res.*, *73*, 267.

Scudder, J. D., X. Cao, and F. S. Mozer (2000), Photoemission current-spacecraft voltage relation: Key to routine, quantitative low-energy plasma measurements, *J. Geophys. Res.*, *105*, 21,281.

Shinohara, M., et al. (1997), Wave characteristics of daytime and nighttime Pi 2 pulsations at the equatorial and low latitudes, *Geophys. Res. Lett.*, *24*, 2279.

Shinohara, M., et al. (1998), Wave characteristics of geomagnetic pulsations across the dip equator, *J. Geophys. Res.*, *103*, 11,745.

Shiokawa, K., et al. (1998), High-speed ion flow, substorm current wedge, and multiple Pi2 pulsations, *J. Geophys. Res.*, *103*, 4491.

Southwood, D. J. (1974), Some features of field line resonances in the magnetosphere, *Planet. Space Sci.*, *22*, 483.

Stuart, W. F. (1974), A mechanism of selective enhancement of Pi2's by the plasmasphere, *J. Atmos. Terr. Phys.*, *36*, 851.

Sutcliffe, P. R. (1975), The association of harmonics in Pi 2 power spectra with the plasmapause, *Planet. Space Sci.*, *23*, 1581.

Sutcliffe, P. R., and L. R. Lyons (2002), Association between quiet-time Pi2 pulsations, poleward boundary intensifications, and plasma sheet particle fluxes, *Geophys. Res. Lett.*, *29*(9), 1293, doi:10.1029/2001GL014430.

Sutcliffe, P. R., and K. Yumoto (1989), Dayside Pi2 pulsations at low latitudes, *Geophys. Res. Lett.*, *16*, 887.

Takahashi, K., S. Ohtani, and B. J. Anderson (1995), Statistical analysis of Pi 2 pulsations observed by the AMPTE CCE spacecraft in the inner magnetosphere, *J. Geophys. Res.*, *100*, 21,929.

Takahashi, K., B. J. Anderson, and K. Yumoto (1999), Upper atmosphere research satellite observation of a Pi2 pulsation, *J. Geophys. Res.*, *104*, 25,035.

Takahashi, K., S.-I. Ohtani, W. J. Hughes, and R. R. Anderson (2001), CRRES observation of Pi2 pulsations: Wave mode inside and outside the plasmasphere, *J. Geophys. Res.*, *106*, 15,567.

Takahashi, K., K. Liou, and K. Yumoto (2002a), Correlative study of ultraviolet aurora and low-latitude Pi2 pulsations, *J. Geophys. Res.*, *107*(A12), 1417, doi:10.1029/2002JA009455.

Takahashi, K., R. E. Denton, and D. Gallagher (2002b), Toroidal wave frequency at L = 6–10: Active magnetospheric particle tracer exploers/CCE observations and comparision with theoretical model, *J. Geophys. Res.*, *107*(A2), 1020, doi:10.1029/2001JA000197.

Takahashi, K., D.-H. Lee, M. Nosé, R. R. Anderson, and W. J. Hughes (2003), CRRES electric field study of the radial mode structure of Pi2 pulsations, *J. Geophys. Res.*, *108*(A5), 1210, doi:10.1029/2002JA009761.

Ulrich, T. J., and T. N. Bishop (1975), Maximum entropy spectral analysis and autoregressive decomposition, *Rev. Geophys.*, *13*, 183.

Yeoman, T. K., and D. Orr (1989), Phase and spectral power of mid-latitude Pi 2 pulsations: Evidence for a plasmaspheric cavity resonance, *Planet. Space Sci.*, *37*, 1367.

Yeoman, T. K., D. K. Milling, and D. Orr (1990), Pi2 pulsation polarization patterns on the U. K. sub-auroral magnetometer network (SAMNET), *Planet. Space Sci.*, *38*, 589.

Yumoto, K. (1986), Generation and propagation mechanisms of low-latitude magnetic pulsations: A review, *J. Geophys. Res.*, *60*, 79.

Yumoto, K., et al. (1994), Correlation of high- and low-latitude Pi2 magnetic pulsations observed at 210° magnetic meridian chain stations, *J. Geomagn. Geoelectr.*, *46*, 925.

Yumoto, K., et al. (1996), The STEP 210° magnetic meridian network project, *J. Geomagn. Geoelectr.*, *48*, 1297.

K.-H. Kim and D.-H. Lee, Department of Astronomy and Space Science, Kyung Hee University, Yongin, Kyunggi, 449-701 Korea. (khan@khu.ac.kr; dhlee@khu.ac.kr)

P. R. Sutcliffe, Hermanus Magnetic Observatory, P.O. Box 32, Hermanus 7200, South Africa. (psutclif@csir.co.za)

K. Takahashi, Johns Hopkins University Applied Physics Laboratory, 11100 Johns Hopkins Road, Laurel, MD 20723-6099, USA. (kazue.takahashi@jhuapl.edu)

K. Yumoto, Space Environment Research Center, Kyushu University, 53 6-10-1 Hakozaki, Fukuoka, 812-8581, Japan. (yumoto@serc.kyushu-u.ac.jp)